

The $J_1...J_3$ method for linear readout of dynamic phase change in a flextensional piezoelectric actuator

Luiz A. P. Marçal, Ricardo T. Higuti, Cláudio Kitano, Emílio C. N. Silva¹

Department of Electrical Engineering, Universidade Estadual Paulista – UNESP, 15385-000, Ilha Solteira, S.P., Brazil, Tokio@dee.feis.unesp.br.

¹Department of Mechatronics and Mechanical Systems Engineering - Escola Politécnica da Universidade de São Paulo, P.O. BOX 31, 05508-900, São Paulo, S.P., Brazil .

Abstract: A new improved version of the $J_1...J_4$ interferometric method for optical phase measurements, named $J_1...J_3$ method, is described, which is of easier implementation and is more stable to phase drift than the original one. This new spectrum technique is used to characterize a flextensional piezoelectric actuator by measuring its nanometric displacement amplitudes.

Key words: Piezoelectric flextensional actuator, interferometry, nanometric displacement measurements.

A. Introduction

Piezoelectric ceramics such as PZT can convert electrical energy to mechanical form. Because of the free strain or displacement (in plane: d_{31} ; out of plane: d_{33}) of the piezoceramics is small, they generally cannot be used directly as actuators in their raw form; consequently, amplification is required. Compliant mechanisms are generally used as mechanical displacement amplifiers to prevent displacement losses that can occur in conventional pin-jointed mechanisms. One kind of this transducer is the piezoelectric flextensional actuator (PFA), which consists of three parts: the metal caps or shell, the active piezoelectric element, and an epoxy adhesive. A schematic of a PFA is shown in Fig. 1: the caps convert and amplify the small radial displacement of the piezoceramic into a much larger axial displacement normal to the surface of the caps. Recently, novel models of optimized PFAs have been designed using the topology optimization technique, a computational design method that combines finite element method and an optimization algorithm [1]. In the present work, a prototype based on these novel flextensional piezoactuators is manufactured and analyzed.

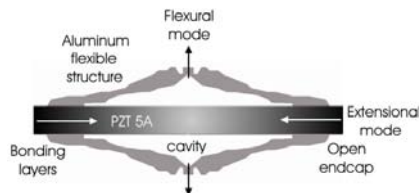


Fig.1. Schematic of the piezoelectric flextensional actuator.

B. The $J_1...J_4$ interferometric method

Optical interferometry provides a convenient technique for measuring displacements in the nanometric and micrometric scales. However, since fluctuations in

ambient temperature and pressure randomly affect the path difference between the two beams of the interferometer, the detected signal undergoes fading. The heterodyne and active homodyne approaches offer attractive ways to eliminate signal fading [2]. Methods of spectrum analysis of the interferometric output can be used to measure displacements by simple passive phase-detection schemes. The technique named $J_1...J_4$ method provides a self-consistent, linear phase readout without using any feedback or phase-bias [3].

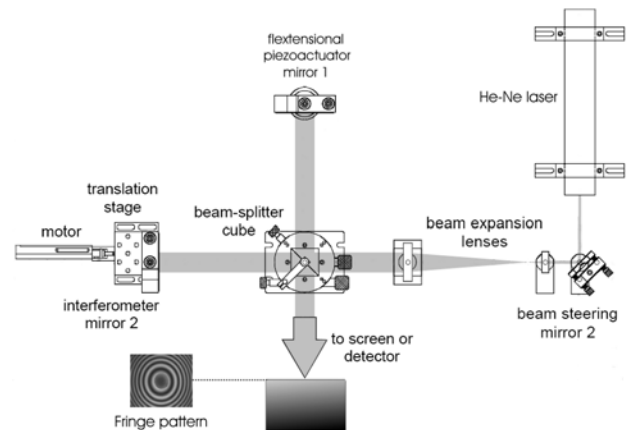


Fig.2. Homodyne Michelson interferometer used to characterize the flextensional piezoactuator.

In this work a low cost Michelson interferometer is employed in the measurement of PFA displacements, as sketched in Fig. 2. A 50/50 beam splitter divides a 5 mW Helium-Neon laser beam ($\lambda=0.6328 \mu\text{m}$) into two equal components: a reference beam and a sensor beam directed towards the fixed and the moving mirrors, respectively. After back reflections, the two beams are recombined at the photodetector. As the sample is displaced longitudinally, the phase of the sensor beam changes relative to the reference beam, causing a fringe pattern movement. By detecting the light intensity at the sensor output, the electric voltage can be estimated from [2]:

$$I(t) = I_0 \{1 + F \cos [\phi_0 + \phi(t)]\} / 2, \quad (1)$$

where I_0 is the laser optical intensity and F is the fringe contrast or visibility. The term ϕ_0 refers to the static phase difference between the sensor and reference beams in the interferometer, and $\phi(t)$ is the phase related to the applied voltage to be measured. When the PFA is excited with a sinusoidal voltage $v(t) = V_{\text{peak}} \sin(\omega_s t)$, with amplitude V_{peak} and angular frequency ω_s , the signal phase-shift can

be written as $\phi(t) = x \sin(\omega_s t)$, where x is the modulation index or amplitude of the phase change. The PFA vibration amplitude or surface displacement at the measurement point is given by $\Delta L = \lambda x / 4\pi$, where λ is the light wavelength.

The sensor output (1) is a non-linear function of the optical phase shift induced by the PFA drive voltage. In addition, the phase ϕ_0 should ideally remain constant, but in practice it is susceptible to signal fading. The non-linear phase-intensity relationship and the signal fading would severely limit the direct applicability of the sensor system. For this reason, adequate techniques must be applied to obtain a linear relationship between output electrical signal and induced phase-shift. Spectrum-analysis techniques can be used as passive phase detection schemes. In this case the photo-detected voltage (1) is written as:

$$I(t) = A + B\{Q[J_0(x) + 2J_2(x)\cos 2\omega_s t + \dots] - P[2J_1(x)\sin\omega_s t + 2J_3(x)\sin 3\omega_s t + \dots]\}, \quad (2)$$

where $A=I_0/2$, $B=I_0F/2$, $P=\sin\phi_0(t)$, and $Q=\cos\phi_0(t)$. The terms J_m 's are Bessel functions of the first kind and order m . Letting V_m be equal to $2BPJ_m(x)$ or $2BQJ_m(x)$, for odd or even values of m , respectively, this technique makes use of the fundamental frequency and its next three harmonics to calculate the dynamic phase modulation index (x) directly, based on the Bessel recurrence relation:

$$x^2 = 24 J_2 J_3 / [(J_1 + J_3)(J_2 + J_4)]. \quad (3)$$

By substituting each $J_m(x)$ in (3) for the corresponding voltage component V_m , the modulation index can be measured. The fading terms P and Q in V_m are cancelled, justifying why phase measurement is unaffected by random phase drifts, source instabilities and changes in visibility. Exception cases must be pointed out, for $\phi_0 = 0$ or $\pi/2$ rad, when P or Q becomes null, and (3) is indetermined. In these cases, it is recommended to proceed to new measurements.

As the modulation index becomes larger, each $J_m(x)$ becomes negative over definite regions of x . Because a spectrum analyzer displays only the magnitudes of spectral components, the incorrect choice of sign could lead to error in the calculation of x^2 . Equation (3) should be suitably corrected for negative signs of $J_m(x)$ by applying, for example, the modified $J_1\dots J_4$ method [4].

It is important to stress that the use of the $J_1\dots J_4$ technique requires that the harmonics magnitudes should be larger than the noise floor at their respective frequencies. So, phase modulation indexes greater than 0.175 rad are needed for a typical interferometric setup [3]. On the other hand, when $x=5.14$ rad there are large errors because $J_1=-J_3$, and both the numerator ($J_2=0$) and the denominator in (3) become zero. So, the $J_1\dots J_4$ method has a dynamic range that is continuous from 0.175 to 5.14 rad approximately. Sudarshanam & Claus proposed the $J_1\dots J_6$ method, which is also fading immune, considering the voltage amplitudes at the fundamental frequency and the next five harmonics [5]. The $J_1\dots J_{6(\text{pos})}$ method shifts the point of discontinuity in phase measurement up to 6.38 rad, while the $J_1\dots J_{6(\text{neg})}$ method

enhances its accuracy to 0.14 rad. In the present paper, it is reported a new improved version of the $J_1\dots J_4$ method, named $J_1\dots J_3$ method, that simplifies the calculus and overcomes some of the limitations of all previous methods.

C. The new $J_1\dots J_3$ method

The new technique is based only on the fundamental (V_1) and third harmonic (V_3) of the photodetected voltage (2). First, f_{13} and f_{24} are defined as the ratios:

$$f_{13} \equiv \frac{V_1 - V_3}{V_1 + 1,93V_3} = \frac{J_1(x) - J_3(x)}{J_1(x) + 1,93J_3(x)} \quad (4a)$$

and

$$f_{24} \equiv \frac{V_2}{V_2 + V_4} = \frac{J_2(x)}{J_2(x) + J_4(x)}. \quad (4b)$$

In the range $0.001 < x < 5.1$ rad the authors observed that factor f_{24} can be written in terms of f_{13} as the following 6th order polynomial:

$$f_{24} = \sum_{k=0}^6 c_k f_{13}^k. \quad (5)$$

The values of the coefficients c_k (for $k=0, \dots, 6$) are established by using the least squares method, in order to minimize the relative error $(x - x_e)/x$, where x_e is the estimated index obtained by substituting (4 a-b) and (5) in (3), resulting:

$$x_e^2 = 24 \frac{V_3}{V_1 + V_3} \sum_{k=0}^6 c_k f_{13}^k. \quad (6)$$

By using the following coefficients: $c_0 = -7.7743 \times 10^{-1}$, $c_1 = 2.8388 \times 10^{-1}$, $c_2 = -6.9985 \times 10^{-2}$, $c_3 = 4.1655 \times 10^{-3}$, $c_4 = 8.7934 \times 10^{-3}$, $c_5 = -3.0286 \times 10^{-3}$, and $c_6 = -1.3113 \times 10^{-3}$, the relative error $(x - x_e)/x$ is plotted as a function of x in Fig. 3. In the range $0.001 \leq x \leq 5.1$ rad the relative error is limited to 0.01%. The standard error is 0.33 mrad, and the correlation factor is 99.9985%.

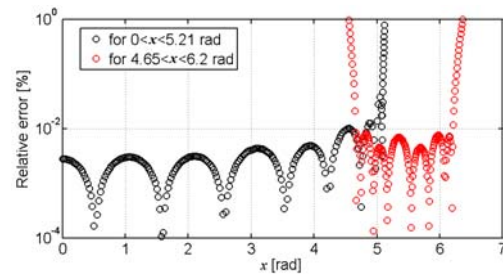


Fig.3. Relative error as function of modulation index x .

The dynamic range of this method can be increased and become equivalent to the $J_1\dots J_{6(\text{pos})}$ method by using another proposed polynomial approximation for x_e , now valid in the range $4.65 < x < 6.21$ rad:

$$x_e = \sum_{k=0}^6 c'_k f_{31}^k \quad (7)$$

and

$$f_{31} = \frac{V_3}{V_1} = \frac{J_3(x)}{J_1(x)}. \quad (8)$$

The coefficients that minimizes the relative error $(x - x_e)/x$ below 0.01% are: $c'_0 = 6.472437$, $c'_1 = 1.729683$, $c'_2 = 4.524875$, $c'_3 = 11.610704$, $c'_4 = 12.179784$, $c'_5 = 5.712492$, and $c'_6 = 1.011324$. This relative error is also plotted as a function of x in Fig. 3. The standard error is 0.246 mrad, and the correlation factor is 99.9979%.

Using (6) and (7) the estimated index x_e only depends on J_1 and J_3 , which constitutes the basis of the new $J_1...J_3$ method. The choice between (6) and (7) can be made by analyzing the value of $g = 1/f_{31}$. As can be seen from Fig. 4(a), for $0.001 < x < 4.83$, $g > -0.78$, and (6) is used, otherwise for $4.83 < x < 6.2$ rad, $g < -0.78$ and (7) is used.

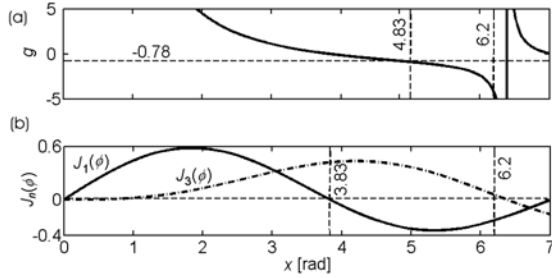


Fig.4. Plots of g and J_1 as function of modulation index x .

While $J_3(x)$ is positive over the range specified above, $J_1(x)$ is negative for values of x greater than 3.83 rad [see Fig. 4 (b)]. In principle, only the algebraic sign of the fundamental component must be considered if the magnitude of the FFT is used. Nevertheless, due to fading, V_1 and V_3 can become negative because P assumes random values between -1 and $+1$. If the signs of both V_1 and V_3 are corrected, the contribution of fading to the final sign are cancelled in the f_{13} and f_{31} relations. When V_1 and V_3 are calculated by the $J_1...J_4$ modified method [4] and applying them in f_{13} and f_{31} , the sign of these harmonics are automatically corrected.

D. Experimental results

In this work, the device designed by topology optimization is shown in Fig. 5, and it consists essentially of a PZT-5A piezoceramic bonded with epoxy to an aluminium flexible structure manufactured by using a wire EDM (Electrical Discharge Machining). The piezoceramic (PZT-5A, American Piezoceramics, 30 mm x 13 mm x 3 mm in directions 1, 2 and 3, respectively) is polarized in direction 3 and electrodes are deposited on the 1-2 plane. PFA displacements decrease away from the centre of the caps, where the maximum displacement is observed, to the edge, where displacement is equal to that of PZT-5A without the endcaps. The flextensional piezoactuator is fixed to a holder (not displayed in figure) by three points, perpendicular to the displacement to be measured. As a reflecting surface is necessary to perform the interferometric measurements, and due to the difficulties to polish the irregular actuator surface to an optical degree, a 200 μm thickness mirror, obtained by aluminum vaporization over a glass plate, was bonded to the actuator surface with epoxy resin (see Fig.5). Additional resonant frequencies that could be caused by

this mirror were not observed (by using an impedance analyser) in the experiments.

The interferometric setup shown in Fig. 2 was built, the PIN photodiode output was amplified, and the signal was digitized by an oscilloscope (Tektronix TDS2022) and transferred to a computer to be post processed. As an example, Fig.6 (a) shows a typical a.c. interferometric output, corresponding to the signal detected when the PFA is driven by a sinusoidal voltage (amplitude of 32 V_{peak} and frequency of 4 kHz). The corresponding Fourier spectrum (in dB) is shown in Fig. 6 (b), where V_1, V_2, \dots are the voltage magnitudes of the spectral components.

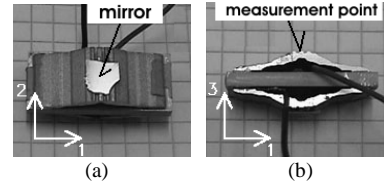


Fig.5. Prototype of manufactured flextensional piezoactuator. a) Top view. b) Lateral view.

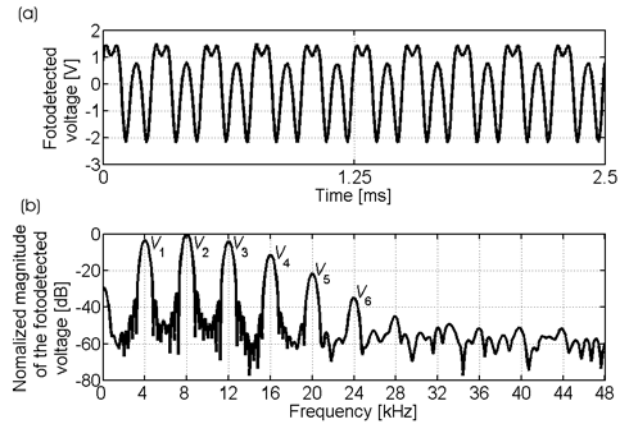


Fig.6. Typical output interferometric signal observed when the PFA is driven with a sinusoidal voltage. a) Photodetected voltage waveform (a.c.). b) The corresponding magnitude spectrum.

For low values of x , J_3 and J_4 become small compared with J_1 and J_2 . So, the values of V_3 and V_4 would be corrupted when they are close to the noise floor at their corresponding frequencies, limiting the sensor dynamic range. Reference [5] established that a $1/f$ noise voltage is a good model for the noise characteristics of these detection methods. In the presence of $1/f$ noise, the modulation index x in (3) must be corrected to x' by substituting each $J_m(x)$ for $[PJ_m(x) + K/m]$ (for m odd) or $[QJ_m(x) + K/m]$ (for m even), where $K = \Delta V_1 / FI_0$, and ΔV_1 is the noise voltage at the fundamental frequency. The factor K can be determined accurately from experiments through an FFT of (1) and depends on the noise characteristics of the specific detector, amplifier, acquisition system and detection bandwidth used. The same substitution must be realized in (4 a) and (8), for f_{13} and f_{31} , respectively. Hence, due to noise the measured value of the a.c. phase shift, x'_e in (6) and (7), deviates from the expected value, x_e . Following the procedure established in [5], the authors measured the value of $K=0.0004$ for the setup shown in Fig.2, at 4-kHz PFA frequency operation.

Figures 7(a) and 7(b) show a 3D-plot of the phase-shift relative errors $\Delta x = (x'_c - x)/x$ and $(x' - x)/x$ as a function of x and $\phi_0(t)$, for the $J_1 \dots J_3$ and $J_1 \dots J_4$ methods, respectively. In order to clarify the graphic discontinuities, the error was limited to 10%. As can be seen in Fig.7, the upper limit of detectable phase shift before a discontinuity occurs is seen to be ~ 6.2 rad for the $J_1 \dots J_3$ method within an error of ± 0.05 rad, which is 16% higher than the upper limit (~ 5.1 rad) for the $J_1 \dots J_4$ method. Based on [5], it concludes that this upper limit is equivalent to that for the $J_1 \dots J_{6(\text{pos})}$ method.

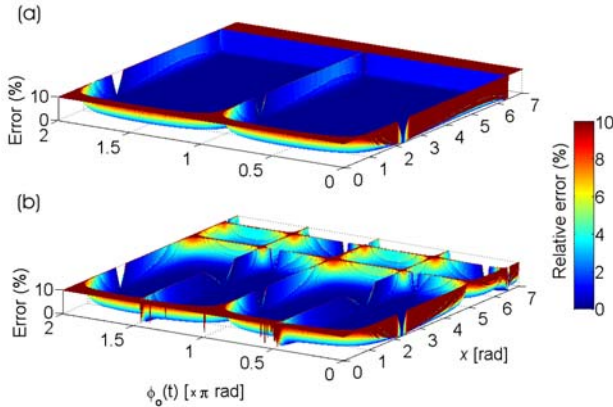


Fig.7. Simulation (for $K=0.0004$) of the relative error in phase-shift as function of expected phase-shift x and random phase-drift $\phi_0(t)$. a) For the $J_1 \dots J_3$ method. b) For the $J_1 \dots J_4$ method.

The minimum detectable phase-shift (MDPS) is defined in [5] as the point at which the plot of Δx versus x intersects the straight line $\Delta x = x$, corresponding to an error of 100%. So, in this condition (not shown in Fig. 7), it was determined that the MDPS for the $J_1 \dots J_4$ and $J_1 \dots J_3$ methods are equivalent (~ 0.18 rad).

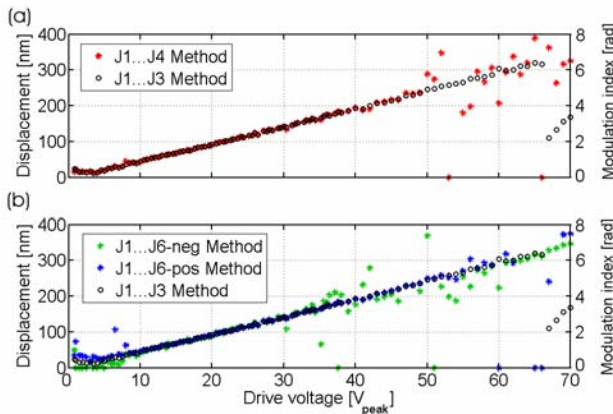


Fig.8. PFA displacement amplitudes measured as function of drive voltage. a) $J_1 \dots J_3$ and $J_1 \dots J_4$ methods. b) $J_1 \dots J_3$, $J_1 \dots J_{6(\text{pos})}$ and $J_1 \dots J_{6(\text{neg})}$ methods.

In order to consider the effect of random phase drift on the measurement of x in (3), it is seen that V_2 and V_4 are zero at $\phi_0 = 90^\circ$, and V_1 and V_3 are zero at $\phi_0 = 0^\circ$. Therefore it is necessary to avoid measurements near $\phi_0 = n\pi/2$ rad, where n is an integer and, as ϕ_0 moves away from these points, the measurement accuracy is increased. This result can be observed in Fig.7(b). By the other hand, Fig. 7(a) reveals that the $J_1 \dots J_3$ method is the least affected by the drift and has the advantage of presenting no discontinuity for odd values of n ,

increasing the global accuracy. All methods give accuracy better than 0.5% at points away from the discontinuities.

Sinusoidal voltages between 0 and 70 V_{peak} were applied to the PFA, obtaining the experimental results shown in Fig.8(a), in terms of displacement amplitudes or modulation index, for the $J_1 \dots J_3$ and $J_1 \dots J_4$ methods; and, in Fig.8(b), for the $J_1 \dots J_3$, $J_1 \dots J_{6(\text{pos})}$ and $J_1 \dots J_{6(\text{neg})}$ methods. As revealed by $J_1 \dots J_3$ method, from 0.14 to 70 V_{peak} drive voltage, the displacement (and the phase-shift) is a linear function of the applied voltage, with a 5 $\text{nm}/V_{\text{peak}}$ coefficient and a 4.5 nm standard deviation.

E. Conclusion

The only spectral components to be measured in the new $J_1 \dots J_3$ method are V_1 and V_3 , while V_2 and V_4 are analytically estimated. Its upper limit of detectable phase shift (within an error of ± 0.05 rad) reaches 6.2 rad, against 5.0, 6.0 and 3.5 rad for the $J_1 \dots J_4$, $J_1 \dots J_{6(\text{pos})}$ and $J_1 \dots J_{6(\text{neg})}$ methods, respectively. Its accuracy (MDPS ~ 0.18 rad with $K=0.0004$) is equivalent to the $J_1 \dots J_4$ (~ 0.175 rad) or $J_1 \dots J_{6(\text{pos})}$ (~ 0.2 rad) methods, but is higher than the $J_1 \dots J_{6(\text{neg})}$ (~ 0.05 rad) method, these last using $K=0.000587$ [5]. So, the $J_1 \dots J_3$ method has the same accuracy and dynamic range of the $J_1 \dots J_{6(\text{pos})}$ method. However, it is the least affected by drift, has no discontinuity at phase quadrature points, and the algebraic sign of the Bessel function can be easier determined. As measurements of higher frequency components are not necessary, the $J_1 \dots J_3$ method demands a smaller sampling rate, reducing system cost and complexity. Also the photodiode bandwidth may be narrowed and the real time operation can be improved.

F. Acknowledgements

The authors would like to thank the Brazilian sponsor agencies FAPESP, CAPES and FUNDUNESP.

G. Literature

- [1] E. C. N. Silva and N. Kikuchi, "Topology optimization design of flextensional actuators," IEEE Transactions on Ultrasonics, Ferroelectrics, and Frequency Control, vol. 47, no. 3, pp.597-605, May 2000.
- [2] L. C. B. Scruby and L. E. Drain, Laser Ultrasonic, Techniques and Applications. Adam Hilger, New York, USA, 1990.
- [3] V. S. Sudarshanam and K. Srinivasan, "Linear readout of dynamic phase change in a fiber-optic homodyne interferometer," Optics Letters, vol. 14, no. 2, pp. 140-142, Jan. 1989.
- [4] W. Jin, L. M. Zhang, D. Uttamchandani, B. Culshaw, "Modified $J_1 \dots J_4$ method for linear readout of dynamic phase changes in a fiber-optic homodyne interferometer," Applied Optics, vol. 30, no. 31, pp. 4496-4499, Nov. 1991.
- [5] V. S. Sudarshanam, R. O. Claus, "Generic $J_1 \dots J_4$ method of optical phase detection-accuracy and range enhancement," Journal of Modern Optics, vol. 40, no. 3, pp. 483-492, Mar. 1993.